Conducting Polymers as Antennas for Probing Biophysical Activities

N. Arun and K. S. Narayan*

Jawaharlal Nehru Centre for Advanced Scientific Research, Bangalore 560 064, India

Received: September 4, 2007; In Final Form: November 4, 2007

Conducting polymers can serve as soft electrode substrates for anchoring and orientating functional membrane proteins. We utilize this possibility to orient bacteriorhodopsin (bR), a membrane protein that functions as a light-driven proton pump, on these substrates. The underlying polymer substrate becomes optoelectronically active with the spectral and temporal characteristics corresponding to that of the adjacent bR molecular layer. We demonstrate the concept of passive and active biomolecular signal transduction using model conducting polymers. The photoinduced current modulation in the conducting polymer layer can be explained in terms of the charge displacements within the proximal bR layer or charge-transfer processes across the interface. We explore the implications of this strong coupling between the photophysical processes in bR and electrical processes in the conducting polymer layer.

Introduction

Conducting polymers have been successfully incorporated in a variety of devices ranging from LEDs, PVs, and FETs.[1−3] The combination of significant electrical properties and the ease of processing these materials has led to their use in versatile applications such as sensors, actuators, and radio frequency identification tags.[4−6] The control of electronic properties and the soft nature of these polymers make them ideal candidates to act as templates for various biological activities.[7,8] The introduction of ion modifies the conductivity of the polymers by a redox reaction, which is associated with "doping", by which the electrochemical potential or the Fermi level is moved into a region of energy where there is a high density of electronic states, with the charge neutrality being maintained by the introduction of counterions.[9] This feature of conducting polymer systems observed in poly(3,4-ethylene dioxythiophene) (PEDOT), polyaniline (PANI), and polypyrrole has been used for various sensing activities. The ion to electron converting action prevalent in organic electrochemical transistors (OECTs) was demonstrated nearly two decades ago and has been utilized to sense water vapor, glucose, and deoxyribonucleic acid.[4,10−12] Recently, various analytes were sensed with these OECTs integrated with bilayer lipid membranes.[13] The transistor action has been explained in terms of an ion-leveraged transport mechanism[14,15] or electrochemical processes.[16,17] Ion channels control the electrical properties of cells by gating in response to a wide array of stimuli. To date, ion channels have been identified that are sensitive to changes in the concentration of ligands such as small molecules and ions, changes in membrane potential, temperature fluctuations, alterations in membrane tension, and exposure to visible light.[18] The prospect of having a smart-electrode interface provides a valuable gateway to monitor and control biological events. The possibility of linking well-defined and patterned organic electronic circuits to cellular activities has immense potential in applications ranging from nervous system to routine chemical sensing.[19,20] We explore the possibility of optically triggering changes in the conductivity of the conducting polymers in contact with the extracellular segments of a membrane protein, bacteriorhodopsin (bR).

bR, a channel protein existing in the halobacterial purple membrane (PM), is a light-driven pump system, sets up an electrochemical gradient, and transports protons across the cell membrane.[21−24] In the "light-adapted" initial B-state, the retinal chromophore, which is the optically active component of the protein, is in an all trans-molecular configuration[24] and has a broad absorption centered around 570 nm. Upon photon absorption, the retinal undergoes configurational and conformational changes and initiates a photocycle, with a net dislocation of the protons from the cytoplasmic to the extracellular side.[25] During this photocycle, the chromophore subsequently goes through a series of short-lived intermediates to the deprotonated longest-lived intermediate, M-state, which has an absorption maximum at 412 nm.[24] The M-state can revert back to the initial B-state through thermal relaxation processes or by photochemical processes upon excitation with blue light.[25]

The signatures of these changes upon photoexcitation also appear in the form of a photoelectric signal across the membrane.[26−29] The photoinduced charge density variation in the bulk and the surface (electrode/electrolyte interface) of the PM manifests in the form of a differential photocurrent.[27] These changes can be spectroscopically followed and were observed to correspond to the primary absorption features of the bR ground state and the M intermediate. Results correlating the phototriggered internal events of bR and the pH changes in the vicinity have been well documented.[26,28] The formation of M intermediate (resulting in increase of proton concentration at the electrode/electrolyte interface due to proton release of bR) has its signature in form of an upward spike of the differential response of the current when the light is switched on, while the decay of M intermediate (which results in a decrease of proton concentration at the interface due to proton uptake of bR) contributes to the light-off photocurrent or the downward spike.[28] These photoelectric signal characteristics measured across the membrane layer can also be modeled in terms of capacitive and resistive components.[29] Another feature that is relevant to the present studies is the process of a reverse proton translocation resulting in the opposite polarity of the photo-

* Corresponding author. E-mail: narayan@jncasr.ac.in.

10.1021/jp077084j CCC: $40.75
Published on Web 01/15/2008

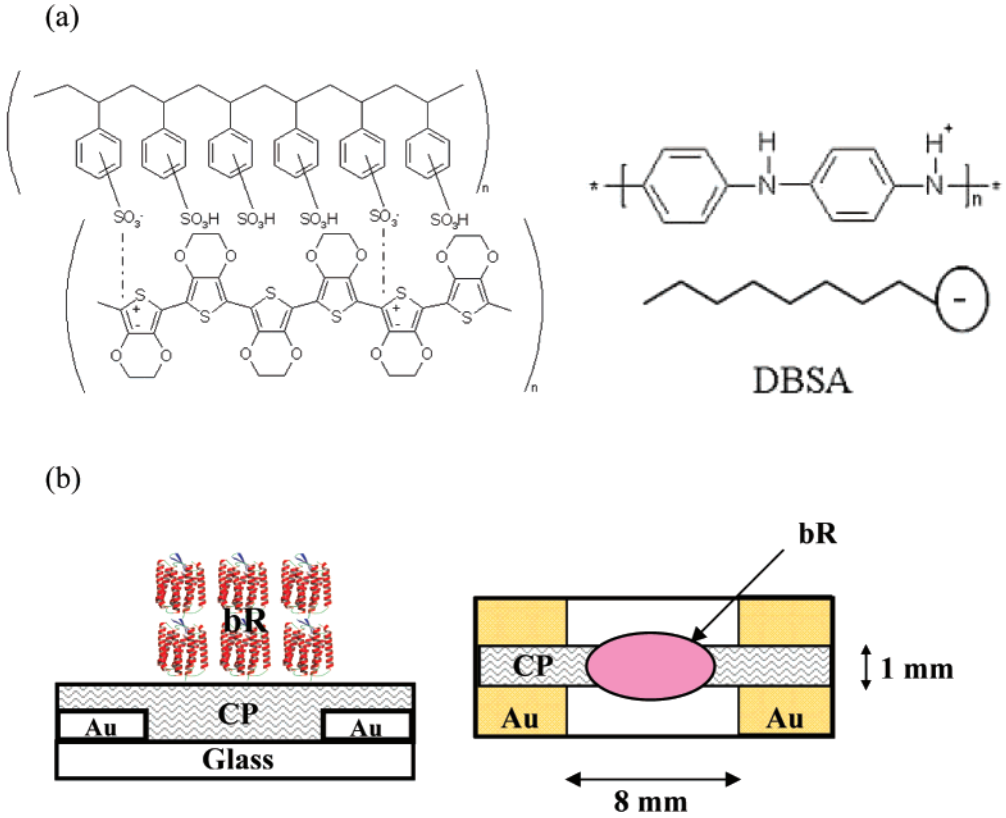

Figure 1. (a) Structure of the polymers used: PEDOT:PSS and PANI:DBSA. (b) Detailed schematic of the device.

voltage (current) during the back-photo reaction upon illuminating the M-state with blue light.[30] The efficiency of extracting and the characteristics of the photoelectric signal are controlled by the external environment, since the limiting factors include the electrochemical reaction kinetics at the bR−electrode interface. The lifetime of the M-state in bR depends on the kinetics of the reprotonation process and can be altered by different means such as controlling the extent of drying, pH conditions, and temperature, and modifying the molecular structure by genetic mutation.[31−33]

bR in conjunction with conducting polymers forms a synergistic pair and highlights several interesting phenomena.[34,35] Earlier results from our laboratory involving bR−conducting polymer structures in the form of solid-state two-terminal sandwich devices using an ITO substrate and top Al electrode revealed distinct enhanced photoelectric signals, and the spectral and temporal characteristics depended on the polarity of the bR−polymer interface.[34] The spectral features of these bias-dependent signals in these sandwich structures were interpreted in terms of the intermediate states appearing in the bR photocycle.[34] The ability of the polymer layer to enhance the photoelectric signal of bR was observed. However, it was not very clear whether the polymer acted as a mere buffer layer or took an active part in the photoelectric process. In this article, we present a correlation between the bR photoelectric signal and the modification in the polymer layer by measuring its conductivity in the three-terminal configuration (insets of Figures 2a and 3a). The conductance modulation of the polymer layer was directly correlated to the photoinduced activities within the bR molecule.

Experimental Details

Gold (Au) strips were thermally evaporated to form an interelectrode gap of 8 mm on precleaned glass substrate. PEDOT:PSS (Baytron P) (Figure 1a) and PANI:DBSA (Panipol W) (Figure 1a) were spin-coated uniformly on these substrates to obtain 100-nm-thick films and then were thermally annealed. PEDOT:PSS, commercially available as Baytron P, was filtered to obtain homogeneous solution, which was then spin-coated on the Au-coated glass substrate. These films were thermally annealed at 140 °C for 1 h to obtain good quality uniform PEDOT:PSS films. PANI:DBSA, commercially available as Panipol W, was diluted using 1:1 ratio of water and polymer and used for spin-coating purposes. Thermal annealing was done at 120 °C for 10 min. Twenty-five microliters of aqueous suspension of bR (MIB, 10 mg/mL) was deposited on the center (5-mm diameter) of the polymer film. A procedure involving a bias potential across the droplet to orient bR (∼200-nm thickness) on substrates during the drying stage was used to form the bR−conducting polymer structures. It is speculated that the anionic component in the polymer blends that forms the surface layer of the film assists the orientation process. An Al layer (<bR dimensions) was then evaporated on the bR on some of the devices. The schematic of the device is shown in the insets of Figures 2a and 3a.

The DC photoelectric response of the structures was measured using a Keithley source meter (model 2400) and a Keithley electrometer (model 6512) interfaced with a computer and was plotted as difference in the DC value between the DC value in presence of light and dark DC value. Different light sources such as laser at $\lambda = 405$ and 532 nm were used. Time-resolved experiments (milliseconds to seconds) were carried out using a standard DC electrometer (Keithley 6514). For the lateral structures without the top Al electrodes, both electrodes were connected to an amplifier (EG&G, current to voltage amplifier) whose output was connected to the electrometer. Photoelectric spectral responses ($V_{ph}(\omega)$) were measured using a lock-in technique, where the output of the 150 W tungsten lamp (Oriel)

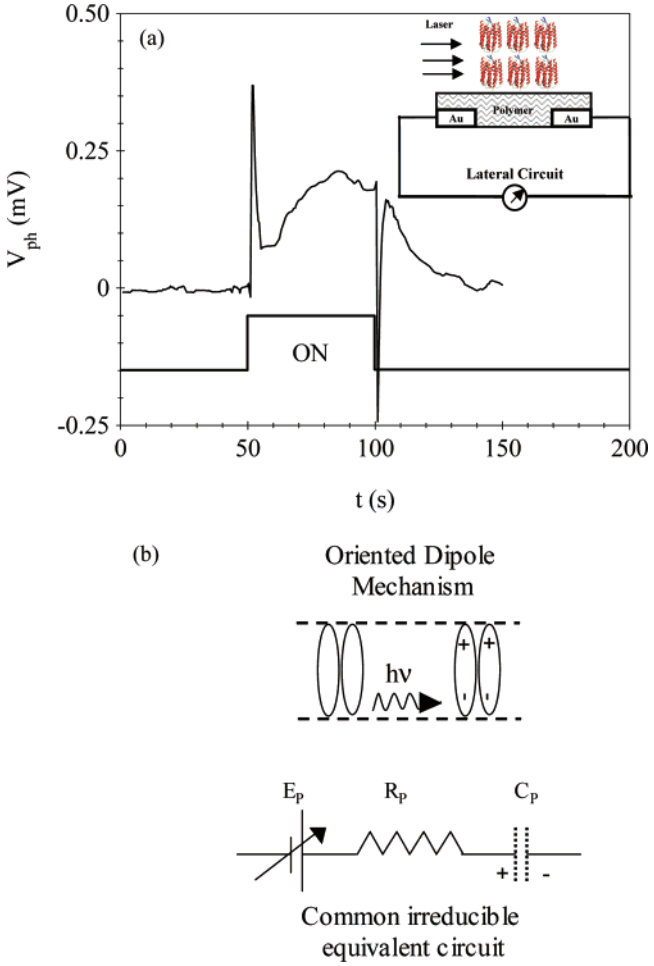

Figure 2. (a) Photoelectric response across the lateral Au electrodes. The lateral DC (V_{Au-Au}) transient response to a light source (532 nm, 1 mW/cm^2) along the PEDOT strip, without the top Al electrode. Inset shows the device schematic. (b) The oriented dipole mechanism. The photoelectric signal is a manifestation of charge separation during the formation of a transient array of electric dipoles.

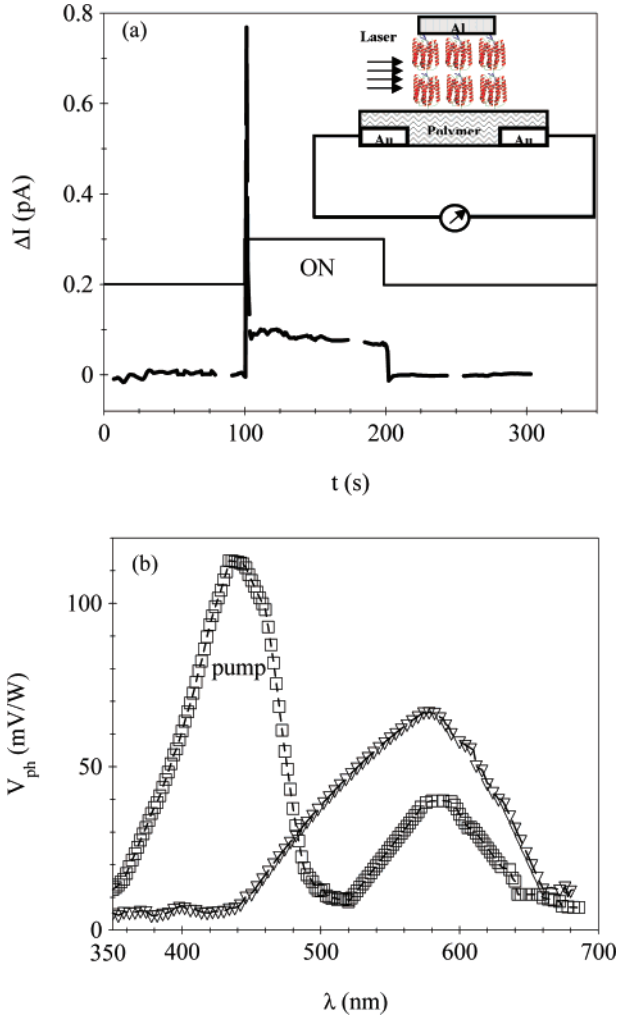

Figure 3. (a) Photoelectric response across the lateral Au electrodes. The lateral, short-circuit DC (I_{Au-Au}) transient response to a light source (532 nm, 1 mW/cm^2) along the PEDOT strip, with the top Al electrode floating. Inset shows the device schematic. (b) Spectral response V_{ph}-(λ) (measured using lock-in technique, $w = 18$ Hz) across the lateral Au electrodes (Al − floating).

was coupled to a monochromator (Acton Research Corporation, SpectraPro 150) that was modulated using a chopper (Stanford Research Systems (SRS), $\omega = 4$ to 400 Hz) and was allowed to incident on the sample. The steady-state intensity-modulated photoelectric response, ($V_{ph}(\omega)$), of the sample was measured using a lock-in amplifier (SRS, model SR830DSP). The photoelectric response was also measured with a pump beam of continuous wave at $\lambda = 532$ nm. Light levels of low intensity (1 mW/cm^2) were used to minimize thermal effects.

Results and Discussion

A clear feature of the interplay between bR and the polymer layer was the striking presence of a photoelectric signal (0.5 mV, 10^8 amplification from a current to voltage preamplifier) between the two lateral Au electrodes bridging the PEDOT:PSS polymer film (Figure 2a inset) even in the absence of any external bias in the circuit. This transient signal/spike characteristic resembled (Figure 2a) that of a typical bR differential response.[36] The local bR origin of these signals was also verified by carrying out measurements on plain polymer structures without bR where the signal was absent. A spatial profile carried out by scanning the light source locally on the PEDOT:PSS strip confirmed the bR origin of the signal in the circuit (Supporting Information). The V_{ph} signal was linear with respect to intensity (1 μw to 1 mW range). It is interesting to observe that the internal photoelectric processes occurring within bR can be probed in a nonintervening manner by monitoring the signal in the adjacent polymer circuit.

The introduction of Al electrode on the bR patch (Figure 3a inset) further enhances the lateral signal across the Au terminals (I_{Au-Au}). The lateral short-circuit ($I(t)_{Au-Au}$) transient signal with Al electrode floating expectedly revealed characteristics analogous to the transmembrane bR differential response (Figure 3a). The photoelectric response spectrum, $V_{ph}(\lambda)$, across the Au electrodes clearly corresponds to the bR ground state (570 nm) (Figure 3b, ▽). Upon additionally pumping the sample, a spectral weight transfer from the ground state (B-state) to the intermediate M-state (410 nm) was observed (Figure 3b, □) giving a quantum efficiency of 74% for the B to M conversion for a pump beam at $\lambda = 532$ nm with 1 mW/cm^2 power density. The presence of a gate-type Al electrode assists in increasing the local electric field as well as contributing to the back-reflected light intensity.

The spectral and the temporal features can be understood using two-level kinetic model consisting of the ground state of bR (B) and the intermediate state (M). We assume that the rate of forward reaction from B to M is k_B, the rate of backward reaction is limited only by the lifetime of M (τ_m) for a simple

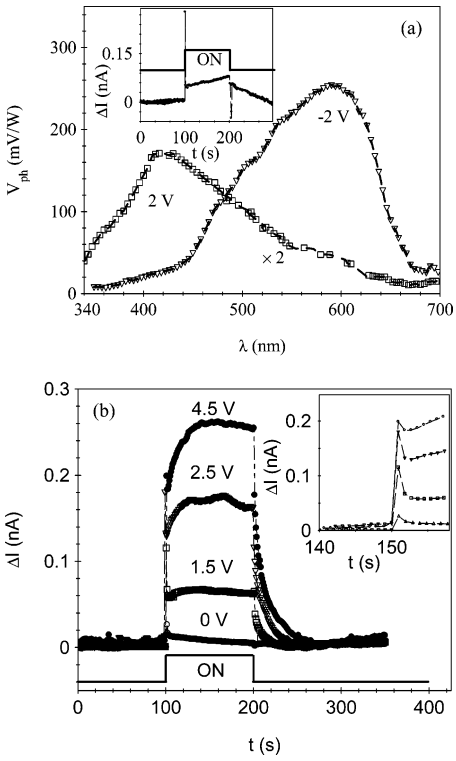

Figure 4. (a) Transverse $V_{ph}(\lambda)$ measured between Al and shorted Au electrodes. Pump laser: 532 nm, 1 mW/cm^2. Inset shows the transverse $\Delta I_{Au,Au-Al}$ upon photoexcitation across the shorted bottom Au electrodes and the top Al electrode. (b) Transient response $\Delta I(t)_{Au-Au}$ (V_{Au-Au} = 0.5 V) of a three-terminal PEDOT/bR device upon photoexcitation (532 nm, 1 mW/cm^2) at different V_{Al-Au}. Inset reveals spike in $\Delta I(t)$ rise.

first-order reaction, and the number of molecules at time t in the ground state after photoexcitation is[37]

$$N_B(t) = \frac{N_T}{k_B + \frac{1}{\tau_M}}\left(\frac{1}{\tau_M} + k_B \cdot \{e^{-[k_B+(1/\tau_M)]\cdot t}\}\right)$$

where the total number of molecules $N_T(t) = N_B(t) + N_M(t)$ and at $t = 0$, $N_M = 0$. k_B is dependent on the light intensity and its wavelength. After we turn off the light, the M-state returns thermally to the initial B-state given by $N_M(t) = N_M(SS)\exp(-t/\tau_M)$ where $N_M(SS)$ is the intensity-dependent, steady-state distribution of M-state molecules. The general microscopic picture of the current induced by photoexciting bR can be attributed to the charge motion of the retinyl chromophore that effectively causes changes in its dipole moment.[27] The orientation of the dipole moments due to photoinitiation of bR causes a time-varying electric and magnetic field in space (Figure 2b). The conducting polymer antenna picks up these variations in the form of displacement currents across its lateral electrodes (similar to the conventional metal antenna). The transduction parameters are dependent on the extent of interaction and are inherently lossy. The polymer layer acts like a microstrip line, picking up the charge fluctuations in bR upon photoexcitation.

The presence of Al electrode can also be utilized to probe the transverse process across the bR−conducting polymer interface by measuring the signal across the top Al electrode and the shorted bottom Au electrodes. Sizable DC photoelectric bR signal across $I_{Au,Au-Al}$ was observed even in absence of an external bias (Figure 4a inset). The $V_{ph}(\lambda)$ measured between the shorted Au electrodes and the top Al electrode emphasizes the bR origin of the photoelectric signals in lateral circuit. Upon applying an additional bias to the top Al electrode, the photoelectric signals were further enhanced because of the contribution from the bulk of the bR and the photoelectric response (Figure 4a) approached that of a two-terminal diode (sandwich) configuration where the bottom electrode is the PEDOT layer. Measurements in this configuration with bias converge to the earlier observations on the two-terminal devices, where the polymer and bR layer were sandwiched between an ITO and Al electrodes.[34] In, the present case, the difference is the marginally lower magnitude of the photosignal due to a signal drop laterally across the conducting polymer layer (∼200 MΩ) compared to the earlier report[34] where the drop was transverse (20 Ω).

An unanswered question in the earlier studies was the effect of the resistive component (the ion motion to electron conversion across the interface) of the signal on the conducting polymer layer. To understand interfacial processes, we study the changes in the conducting polymer layer upon photoexciting bR by monitoring the lateral conductance ($I(t)_{Au-Au}$) of the polymer layer (V_{Au-Au} = 0.5 V). An important point of note is that the application of only the Al-gate bias without any photoexcitation did not cause any electrochemical change (de-doping) in the polymer layer, that is, the conductivity of the polymer (within 5%) is not modified. In the dry bR patch, the structurally bound and the relatively low concentration of residual water molecules[38] are not sufficient to promote electrochemical reduction of PEDOT:PSS. Upon photoexcitation, an asymmetric response was observed (Figure 4b) suggesting a preferred direction of H^+ displacement (toward the polymer layer). The signal changed from differential at V_{Al-Au} = 0 V gradually to a resistive character at higher positive (+Al) voltages (Figure 4b). However, upon removal of the photoexcitation, the conductance changes did not persist and the conductivity of the polymer layer reverted to its original value (Figure 4b). Upon terminating the photoexcitation, the exponential decay of the current was modeled in terms of the diffusion of the protons in bR, $I \propto A\exp(-t/\tau)$ with a single time constant that increased with the applied bias (8.4, 11.9, and 14.6 s for 1.5, 2.5, and 4.5 V, respectively). The time constants observed in these cases were similar to the ones observed by MacDiarmid et al. and Epstein et al. in their field effect transistors based on PEDOT:PSS as the active material.[14,15] The transient profiles, indicating differential nature of the photoinduced current and the $V_{ph}(\lambda)$, corresponding to the bR signatures in both the configurations clearly reveal the interplay between the lateral and transverse processes.

On the basis of this set of observations, it is speculated that the initial spike in the lateral signal across the PEDOT strip arises from the change of dipole moment within the adjacent layer of bR molecules upon photoexcitation.[39] The change in the dipole moment induces an electric field that modifies the interface potential between bR and the PEDOT:PSS layer. These changes in the surface potential of bR temporarily modify the local transport pathways in the PEDOT:PSS layer that in turn results in a transient change in the conductivity of the polymer layer. Other factors that may influence include photoinduced ionic leakage and thermal effects, which are small in the present case.[40] No *permanent* change in conductivity of the PEDOT:PSS layer was observed after the light exposure experiment on the bR patch. Experimental observations do not point to the possibility of H^+ reducing PEDOT:PSS or compensating PSS^-.[16,17] The surface morphology and the electrical transport characteristics of PEDOT:PSS appear to be a factor for observing the photoelectric features. Dried PEDOT:PSS film

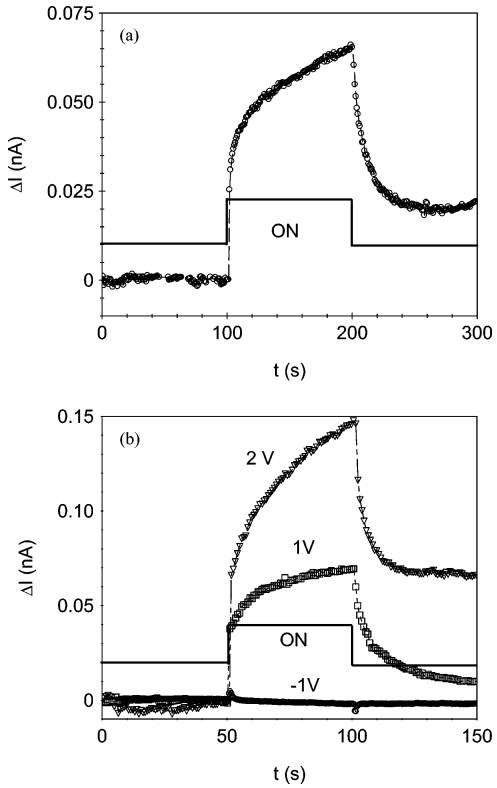

Figure 5. (a) Transverse $\Delta I(t)_{Al-Au}$ upon photoexcitation across the bottom shorted Au electrodes and the top Al electrodes. (b) $\Delta I(t)_{Au-Au}$ ($V_{Au-Au} = 0.5$ V) of a three-terminal PANI/bR device at different V_{Al-Au} upon photoexcitation (532 nm, 1 mW/cm^2).

in its pristine form is known to phase segregate with the surface richer in PSS^- component. Addition of solvent agents such as sorbitol and glycerol results in films with more uniform surface and higher conductivity.[41] The signal transduction was not observed for device structures with the higher conducting form of PEDOT:PSS (blended with glycerol) films. These results point to the importance of the dimensional and impedance matching conditions. Engineering the polymer film surface can then optimize the signal efficiencies.

In the case of PANI, it is known that introduction of protonic acids, in addition to controlling the oxidation state, increases the conductivity due to the protonation at the nitrogen site.[42] The acid-based doping mechanism is different from the oxidative doping achieved in other conducting polymer systems.[9,42] PANI:DBSA films are generally aggregated nanoparticles. The hydrophobic tails of free and bonded DBSA molecules are arranged in a way so that they all turn toward each other, while the hydrophilic groups of the free DBSA turn to the surrounding medium.[43] In these nanoparticles, the anilinium cation resides in the shell complexed with sulfate ion. The anilinium cations are oriented with the phenyl moiety toward the core and the NH_3 to the outer side.[44] The excess DBSA acts as surfactant in the solution and plays a role of plasticizer in the film. This represents an appropriate situation for the bR−conducting polymer film interface, where the bR can possibly source protons upon photoexcitation from its environment and transfer them across the interface. The efficiency of this process is likely to be affected in dried films, but signature of this interplay is indicated in the results.

Transient DC measurements of three-terminal device structures based on PANI/bR, between the top Al electrode and the shorted Au electrodes, revealed a direct increase in $I_{Au,Au-Al}$ upon photoexcitation instead of the differential response as observed in PEDOT:PSS/bR structures (Figure 5a). Note that the steady-state frequency domain technique is not suitable to observe these photochemical effects on the PANI surface, since the slow diffusion and reaction process within the polymer films are not correlated to incident photoexcitation rates. It was observed, after carrying out studies on a large number of devices, that the photomodulated lateral signal, which was observed in the case of conducting polymers based on PEDOT:PSS/bR, was absent in the case of PANI/bR. The absence of the steady-state lateral signal as well as in the transverse case can be partially attributed to larger resistance of the polyaniline films, which is greater than an order of magnitude than that of the PEDOT:PSS films for similar device dimensions.

The steady-state photoelectric signal ($V_{ph}(\omega)$) is easily observable in the two-terminal bilayer sandwich structure ITO/PANI/bR/Al structure. The photoelectric features in these devices were similar to that of the pristine bR case (Supporting Information). An important observation in the bilayer structures was the gradual decrease of the steady-state photoelectric voltage ($\lambda = 532$ nm) in magnitude over a period of time (Supporting Information), which can be attributed to the PANI-doping process. This indicates that the photocycle is not completed and the bR is frozen in the M-state. The frozen M-state can be observed in the form of a small steady-state photoelectric signal at $\lambda = 405$ nm. The transitory PANI-doping process implies that the pumped protons are not readily available for reprotonation of the bR molecule leading to a decrease in the bR cycle completion rate and appearing in the form of a slowly decaying V_{ph}.

The results get modified upon introduction of bias to the top Al electrode, with a larger signal for positive bias, whereas in the negative bias the conductance remains unchanged. In the three-terminal device structures involving PANI/bR, the lateral DC I_{Au-Au} ($V_{Au-Au} = 0.5$ V) increased upon illumination, indicating features of active doping of the polymer surface initiated by the bR-proton pumping activity. Upon switching off the light, $I(t)_{Au-Au}$ followed a characteristic decay profile (Figure 5b). Note that the current value after the exposure to a brief duration of light was higher than the initial value (Figure 5b). This residual increase in the conductivity appeared to be a function of the applied transverse voltage (Figure 5b). The decay $I(t)_{Au-Au}$ upon the termination of the photoexcitation followed the double exponential profile, $I \propto A[\exp(-t/\tau_1) + \exp(-t/\tau_2)]$, indicative of two independent processes. The decay parameters and the bias voltage cannot be correlated because of the persistent residual fraction of the current that appears as an additional parameter. The results from these bulk measurements can be attributed to a transient surface doping phenomena, representing only a fraction of conducting polymer film. Additionally, the excess space charge on the polymer due to the proton diffusion-limited process can reduce the efficiency of the doping mechanism. The observation that a voltage bias across the bR patch alone does not activate changes in conducting polymer but requires the appropriate photoexcitation points toward a correlation between the bR photoactivity and electrical property of PANI. The PANI/bR structures provide an example of a hybrid system with the results arising from a combination of interdependent physical processes of each system.

From the biophysical perspective, it is known that proton pumping efficiency of bR in the solid state is reduced.[45,46] The signature of proton displacement in bR upon photoexcitation in different media is well documented. However, the spatial degree of freedom for the proton pumped into the extracellular region is not known in great detail. There have been reports

that indicate rapid pH variation on the surface of bR accompanied by very slow changes in the bulk outside in the medium.[47,48] The existence of $V_{ph}(\lambda)$ features representing the two states (B and M) along with the absence of commensurate nonreversible changes in the polymer indicate a constrained spatial degree of freedom for the proton. The protons are reabsorbed by the retinal chromophore either directly or indirectly through percolating pathways present in the purple membrane, thereby maintaining the charge neutrality.

Factors such as the signal-to-noise and bandwidth in these macrosized structures can be considerably enhanced in the short-channel structures. Recent methods for controlled deposition of bR thin films, coupled with modern technology for fabricating electrodes with very small channel length, can be used to increase the quantum efficiencies of these processes. These lateral electrode-based bilayer structures can also be used to probe various other biomolecular processes in a noninvasive manner without the presence of nonlinear *IV* background processes that are dominant in molecular thin films.

Conclusion

We demonstrate the possibility of efficient signal transduction of a biophysical process in bR to the adjacent conducting polymer layer. Mechanism of the bR*-induced conductance changes in PEDOT:PSS appeared to be different from that of PANI. Steady state measurable electrical signals in the polymer (PEDOT:PSS) circuit represented internal changes of the proximal biomolecule upon photoexcitation. The light-induced dipole fluctuations within bR are translated into conductance changes in the PEDOT:PSS case. A signature of transient doping of the polymer surface due to the proton displacements in the bR system was observed in the PANI:DBSA case, where the surface H^+ concentration changes are picked up by the polymer. This concept of passive and active biomolecular signal transduction can be used to probe the internal processes of the biomolecules and also utilized for various sensing activities.

Supporting Information Available: Time-resolved experiments involving green light followed by blue light, line scan of the device, photoelectric response of ITO/PANI/bR/Al bilayer structure, and steady-state lock-in measurements. This material is available free of charge via the Internet at http://pubs.acs.org.

References and Notes

(1) Brown, T. M.; Kim, J. S.; Friend, R. H.; Cacialli, F.; Daik, R.; Feast, W. J. *Appl Phys. Lett.* **1999**, *75*, 1679−1681.

(2) Dhanabalan, A.; Van Duren, J. K. J.; Van Hal, P. A.; Van Dongen, J. L. J.; Janssen, R. A. J. *Adv. Funct. Mater.* **2001**, *11*, 255−262.

(3) Halik, M.; Klauk, H.; Zchieschang, U.; Schmid, G.; Radlik, W.; Weber, W. *Adv. Mater.* **2002**, *14*, 1712−1722.

(4) Chao, S.; Wrighton, M. S. *J. Am. Chem. Soc.* **1987**, *109*, 6627−6631.

(5) Hutchison, A. S.; Lewis, T. W.; Moulton, W. E.; Spinks, G. M.; Wallace, G. G. *Synth. Met.* **2000**, *113*, 121−127.

(6) Clemens, W.; Fix, W.; Ficker, J.; Knobloch, A.; Ullmann, A. *J. Mater. Res.* **2004**, *19*, 1963−1973.

(7) Xiao, Y.; Cui, X.; Hancock, J. M.; Bouguettaya, M.; Reynolds, J. R.; Martin, D. C. *Sens. Actuators, B* **2004**, *99*, 437−443.

(8) Gaylord, B. S.; Heeger, A. J.; Bazan, G. C. *J. Am. Chem. Soc.* **2003**, *125*, 896−900.

(9) Heeger, A. J. *Rev. Mod. Phys.* **2001**, *73*, 681−700.

(10) Nilsson, D.; Kugler, T.; Svensson, P.; Berggren, M. *Sens. Actuators, B* **2002**, *86*, 193−197.

(11) Zhu, Z.; Mabeck, J. T.; Zhu, C.; Cady, N. C.; Batt, C. A.; Malliaras, G. G. *Chem. Commun.* **2004**, 1556−1557.

(12) Krishnamoorthy, K.; Gokhale, R. S.; Contractor, A. Q.; Kumar, A. *Chem. Commun.* **2004**, 820−821.

(13) Bernards, D. A.; Malliaras, G. G.; Toombes, G. E. S.; Gruner, S. M. *Appl. Phys. Lett.* **2006**, *89*, 053505.

(14) Lu, J.; Pinto, N. J.; MacDiarmid, A. G. *J. Appl. Phys.* **2002**, *92*, 6033−6038.

(15) Epstein, A. J.; Hsu, F.; Chiou, N.; Prigodin, V. N. *Curr. Appl. Phys.* **2002**, *2*, 339−343.

(16) Nilsson, D.; Chen, M.; Kugler, T.; Remonen, T.; Armgarth, M.; Berggren, M. *Adv. Mater.* **2002**, *14*, 51−54.

(17) Chen, M.; Nilsson, D.; Kugler, T.; Berggren, M.; Remonen, T. *Appl. Phys. Lett.* **2002**, *81*, 2011−2013.

(18) Ito, T.; Hioki, T.; Yamaguchi, T.; Shinbo, T.; Nakao, S.-I.; Kimura, S. *J. Am. Chem. Soc.* **2002**, *124*, 7840−7846.

(19) Cui, X.; Martin, D. C. *Sens. Actuators, B* **2003**, *89*, 92−102.

(20) McQuade, D. T.; Pullen, A. E.; Swager, T. M. *Chem. Rev.* **2000**, *100*, 2537−2574.

(21) Stoeckneius, W. *Protein Sci.* **1999**, *8*, 447−459.

(22) Bioelectronic Applications of Photochromic Pigments; Der, A., Keszthelyi, L., Eds.; NATO Science Series, Series 1, Life and Behavioural Sciences 335; IOS Press: Amsterdam, 2001.

(23) Lanyi, J. K. *Annu. Rev. Physiol.* **2004**, *66*, 665−688.

(24) Birge, R. R. *Biochim. Biophys. Acta* **1990**, *1016*, 293−327.

(25) Drachev, L. A.; Kaulen, A. D.; Skulachev, V. P. *FEBS Lett.* **1984**, *2168*, 331−335.

(26) Wang, J.-p.; Song, L.; Yoo, S.-k.; El-Sayed, M. A. *J. Phys. Chem. B* **1997**, *101*, 10599−10604.

(27) Der, A.; Keszthelyi, L. *Biochemistry (Moscow)* **2001**, *66*, 1234−1248.

(28) He, J.; Samuelson, L.; Li, L.; Kumar, J.; Tripathy, S. K. *J. Phys. Chem. B* **1998**, *102*, 7067−7072.

(29) Trissl, H. *Photochem. Photobiol.* **1990**, *51*, 793−818.

(30) Takei, H.; Lewis, A.; Chen, Z.; Nebenzahi, I. *Appl. Opt.* **1991**, *30*, 500−509.

(31) Dyukova, T.; Robertson, B.; Weetall, H. *Biosystems* **1997**, *41*, 91−98.

(32) Hong, F. T. *Prog. Surf. Sci.* **1999**, *62*, 1−237.

(33) Li, M.; Li, B.; Jiang, L.; Tussila, T.; Tkachenko, N.; Lemmetyinen, H. *Langmuir* **2000**, *16*, 5503−5505.

(34) Manoj, A. G.; Narayan, K. S. *Appl. Phys. Lett.* **2003**, *83*, 3614−3616.

(35) Manoj, A. G.; Narayan, K. S. *Biosens. Bioelectron.* **2004**, *19*, 1067−1074.

(36) The direction of the current as measured by the electrometer is governed by the probe terminals. In the electrometer, the center conductor is the high impedance lead while the inner shield is the low impedance one. The inner shield is connected to the chassis ground. This asymmetry introduced by the probe provides the directionality.

(37) Seitz, A.; Hampp, N. *J. Phys. Chem.* **2000**, *104*, 7183−7192.

(38) Stricker, J. T.; Gudmundsdottir, A. D.; Smith, A. P.; Taylor, B. E.; Durstock, M. F. *J. Phys. Chem B* **2007**, *111*, 6322−6326.

(39) Lee, I.; Greenbaum, E.; Budy, S.; Hillebrecht, J. R.; Birge, R. R.; Stuart, J. A. *J. Phys. Chem. B* **2006**, *110*, 10982−10990.

(40) Jin, Y.; Friedman, N.; Sheves, M.; He, T.; Cahen, D. *Proc. Natl. Acad. Sci. U.S.A.* **2006**, *103*, 8601−8606.

(41) Jonsson, S. K. M.; Birgerson, J.; Crispin, X.; Greczynski, G.; Osikowicz, W.; Denier van der Gon, A. W.; Saleneck, W. R.; Fahlman, M. *Synth. Met.* **2003**, *139*, 1−10.

(42) Macdiarmid, A. G.; Chiang, J. C.; Richter, A. F. *Synth. Met.* **1987**, *18*, 285−290.

(43) Haba, Y.; Segal, E.; Narkis, M.; Titelman, G. I.; Seigmann, A. *Synth. Met.* **2000**, *110*, 189−193.

(44) Han, M. G.; Cho, S. K.; Oh, S. G.; Im, S. S. *Synth. Met.* **2002**, *126*, 53−60.

(45) Haupts, U.; Tittor, J.; Osterhelt, D. *Annu. Rev. Biophys. Biomol. Struct.* **1999**, *28*, 367−399.

(46) Varo, G.; Lanyi, J. K. *Biophys. J.* **1991**, *59*, 313−322.

(47) Heberle, J.; Riesle, J.; Thiedemann, G.; Oesterhelt, D.; Dencher, N. A. *Nature* **1994**, *370*, 379−382.

(48) Heberle, J.; Dencher, N. A. *Proc. Natl. Acad. Sci. U.S.A.* **1992**, *89*, 5996−6000.